DELTA-SIGMA MODULATOR TOPOLOGIES WITH HIGH IMMUNITY TO PATTERN NOISE

Godi Fischer and Deokhwan Hyun

Department of Electrical & Computer Engineering
University of Rhode Island
Kingston, RI 02881, U.S.A.
E-mail: fischer@ele.uri.edu

ABSTRACT

This paper addresses the problem of pattern noise encountered in single-stage delta-sigma modulators in the presence of a DC input signal. By utilizing state-space matrices, we explain the cause of these undesired cyclic patterns and show how a modulator's susceptibility to tonal behavior can be determined by inspection of the system matrix **A**. By example of two frequently used single-stage architectures, a 2^{nd} and a 3^{rd} order system, we demonstrate that simple topological modifications can render a given system immune to cyclic sequences. The two examples prove that this immunity can be achieved without visibly degrading the modulator's noise shaping capability. In fact, the modification applied to the 2^{nd} order system even improves the quantization noise suppression.

1. INTRODUCTION

If the input of a single-stage delta-sigma modulator (DSM) remains constant over a sufficiently long time interval or varies very slowly, it is possible that the quantizer output stream becomes cyclic. Such an undesired periodic output pattern generates discrete noise components commonly referred to as tones. Due to the high oversampling rate (OSR), most of these tonal components will be located outside the modulator passband, where they do little harm. However, some cycles will be long enough to leave their signature in the band of interest, i.e, between DC and $f_s/(2\ OSR)$. Typically, the power of the resulting spectral components is very low. However, the human ear is particularly susceptible to discrete tones and their presence can seriously degrade the spurious free dynamic range (SFDR) of the entire system. Low order single-stage DSM's are particularly prone to exhibit tonal frequency components in their output spectrum.

Although great efforts have been applied to analyze the cyclic behavior of these systems [1, 2, 3] and mitigate this performance degrading effect by incorporating dithering schemes [4, 5, 6, 7], there exists no comprehensive analysis procedure for higher order systems, which would allow a designer to predict the spectral distribution of possible limits cycles and their expected power levels.

This paper attempts to shed more light onto this subject by explaining the cause of limit cycles and suggesting some topological modifications that can prevent the occurrence of cyclic patterns altogether.

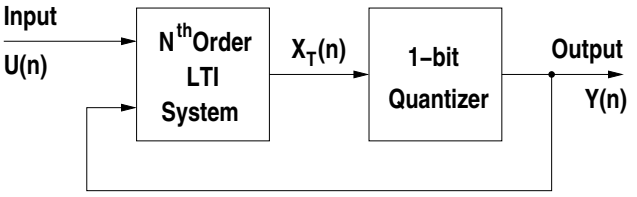

Figure 1: Block diagram of an N^{th} order discrete-time single-bit DSM.

2. CAUSE OF LIMIT CYCLES

Figure 1 shows a simplified block diagram of a discrete-time single-stage DSM topology. If we describe the linear, time-invariant (LTI) block of this discrete-time system in state-space notation, we can express the next state vector by the following matrix equation [8]

$$\mathbf{x}(n+1) = \mathbf{A}\ \mathbf{x}(n) + \mathbf{B}y(n) + \mathbf{C}u(n) \tag{1}$$

where $\mathbf{A}$ represents the N×N system matrix (of an N^{th} order system), while $\mathbf{B}$ and $\mathbf{C}$ denote the N×1 feedback and input vectors, respectively. Since we assume a single-bit quantizer, the output sequence can be written as

$$y(n) = \beta \cdot \text{sgn}[x_T(n)] \tag{2}$$

where x_T represents the quantizer input (generally a weighted sum of state variables) and β specifies the magnitude of the quantizer output, e.g. a fixed reference voltage.

The entire system can now be described by the following set of difference equations

$$\begin{aligned} \mathbf{x}(n+1) &= \mathbf{A}\ \mathbf{x}(n) + \mathbf{B}\beta + \mathbf{C}u(n) && x_T(n) \geq 0 \\ \mathbf{x}(n+1) &= \mathbf{A}\ \mathbf{x}(n) - \mathbf{B}\beta + \mathbf{C}u(n) && x_T(n) < 0 \end{aligned} \tag{3}$$

If $u(n)$ is equal to a constant α, we can rewrite these two difference equations as

$$\begin{aligned} \mathbf{x}(n+1) &= \mathbf{A}\ \mathbf{x}(n) + \mathbf{DP} && x_T(n) \geq 0 \\ \mathbf{x}(n+1) &= \mathbf{A}\ \mathbf{x}(n) + \mathbf{DN} && x_T(n) < 0 \end{aligned} \tag{4}$$

where

$$\begin{aligned} \mathbf{DP} &= \mathbf{B}\beta + \mathbf{C}\alpha & x_T(n) \geq 0 \\ \mathbf{DN} &= -\mathbf{B}\beta + \mathbf{C}\alpha & x_T(n) < 0 \end{aligned} \quad (5)$$

The difference between two successive samples of the state vector $\mathbf{x}(n)$ can be expressed as

$$\begin{aligned} \mathbf{\Delta x}(n) = \quad & (\mathbf{A}-\mathbf{I})\mathbf{x}(n) + \mathbf{DP} & x_T(n) \geq 0 \\ & (\mathbf{A}-\mathbf{I})\mathbf{x}(n) + \mathbf{DN} & x_T(n) < 0 \end{aligned} \quad (6)$$

If the input remains constant over n cycles, we can utilize this recursive formula to express the state vector $\mathbf{x}(n)$ as follows

$$\begin{aligned} \mathbf{x}(n) = \mathbf{A}^n\mathbf{x}(0) &+ (\mathbf{A}^{n-g_1} + \mathbf{A}^{n-g_2} + \ldots)\mathbf{DP} \\ &+ (\mathbf{A}^{n-k_1} + \mathbf{A}^{n-k_2} + \ldots)\mathbf{DN} \end{aligned} \quad (7)$$

The superscripts $n-g_i$ and $n-k_i$ are exponents, which depend on the specific limit cycle sequence. Note that all powers of matrix $\mathbf{A}$ absent in the second term on the right hand side of equation 7 will appear in the third term. If the system is trapped in a limit cycle of length n, vector $\mathbf{x}(n)$ must be identical to its initial value $\mathbf{x}(0)$. We can therefore write

$$\begin{aligned} (\mathbf{I}-\mathbf{A}^n)\mathbf{x}(0) &= (\mathbf{A}^{n-g_1} + \mathbf{A}^{n-g_2} + \ldots)\mathbf{DP} \\ &\quad + (\mathbf{A}^{n-k_1} + \mathbf{A}^{n-k_2} + \ldots)\mathbf{DN} \\ &= \mathbf{x}' \end{aligned} \quad (8)$$

In most practical DSM circuits, matrix $(\mathbf{I}-\mathbf{A}^n)$ turns out to be N-1 dimensional. In this case, matrix $(\mathbf{I}-\mathbf{A}^n)$ is singular and there exist infinitely many solutions for $\mathbf{x}(0)$. In other words, each cyclic pattern possesses *infinitely many initial conditions*. Hence, limit cycles are very likely to occur. If we subject matrix $(\mathbf{I}-\mathbf{A}^n)$ to a singular value decomposition (SVD), we obtain

$$(\mathbf{I}-\mathbf{A}^n) = [\mathbf{U_1}\ \mathbf{U_2}] \begin{bmatrix} \mathbf{\Sigma_1} & 0 \\ 0 & 0 \end{bmatrix} \begin{bmatrix} \mathbf{V_1}^T \\ \mathbf{V_2}^T \end{bmatrix} \quad (9)$$

where $\mathbf{\Sigma_1}$ is an N-1×N-1 diagonal matrix.

The solutions for the initial state vector $\mathbf{x}(0)$ can now be parameterized by a 1-dimensional vector as follows

$$\mathbf{x}(0) = \mathbf{V_1}\mathbf{\Sigma_1}^{-1}\mathbf{U_1}^T\mathbf{x}' + \mathbf{V_2}w \quad (10)$$

where w represents an arbitrary scaling constant, which can be adjusted to find a specific initial condition.

3. TOPOLOGIES WITH HIGH IMMUNITY TO LIMIT CYCLES

In the recent past, several practical solutions have been presented for the prevention of limit cycles. Since these undesired cyclic patters are relatively fragile [8], they can be disrupted and thus terminated by a weak stochastic dither signal [4]. Alternative methods make use of the chaotic nature of a marginal stable DSM loop [5] or alter the system topology [6]. While all these methods can prevent tonal patters, they also penalize the maximum signal to noise plus distortion ratio (SNDR) of the system. In what follows, we will present a solution, which minimizes this penalty or even improves the maximum SNDR.

We have shown in the previous section that cyclic patterns are bound to occur if the difference vector Δx between two consecutive states (cf. equation 6) is less than N-dimensional, in other words, if Δx is restricted to a subspace of the entire state space. For this to happen, matrix $[\mathbf{A}-\mathbf{I}]$ must be of rank N-1 or lower. Conversely, if we find a topology where the rank of matrix $[\mathbf{A}-\mathbf{I}]$ is equal to the system order N, limit cycles become virtually impossible, since equation 8 can be satisfied by exactly one initial state vector $\mathbf{x}(0)$. This unique solution will hardly be encountered in a practical system or may even lie outside the range of practically possible state vectors. Thus, by simply inspecting the rank of matrix $[\mathbf{A}-\mathbf{I}]$, we can predict whether or not a DSM system is likely to suffer from cyclic patterns.

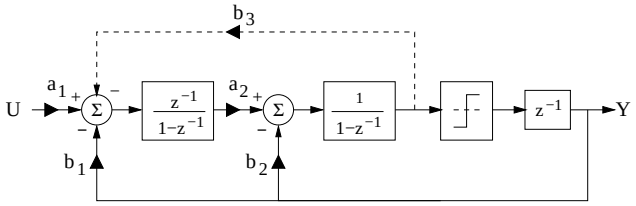

Figure 2: Block diagram of 2^{nd} order DSM with additional feedback b_3 to prevent cyclic output patterns.

To illustrate this crucial point, let us consider the frequently used 2^{nd} order DSM topology depicted in figure 2. If we include the proposed additional feedback path b_3, the $[\mathbf{A}-\mathbf{I}]$ matrix of this system becomes

$$[\mathbf{A}-\mathbf{I}]_2 = \begin{bmatrix} 0 & -b_3 \\ a_2 & -a_2 b_3 \end{bmatrix} \quad (11)$$

Evidently, the additional feedback b_3 keeps the rank of matrix $[\mathbf{A}-\mathbf{I}]_2$ equal to N=2. Tonal patterns should therefore rarely occur. As far as the noise noise shaping property of this modulator is concerned, b_3 can even be beneficial, since the double integrator loop, comprising the coefficients b_3 and a_2, realizes a finite passband zero. To minimize the passband quantization noise power, the gain of this zero loop should be chosen as

$$g_{02} = a_2 b_3 = \frac{1}{3}\frac{\pi^2}{OSR^2} \quad (12)$$

If the coefficient product $a_2 b_3$ satisfies equation 12, the quantization noise should be suppressed by an additional factor of 9/4 or 3.5 dB, respectively.

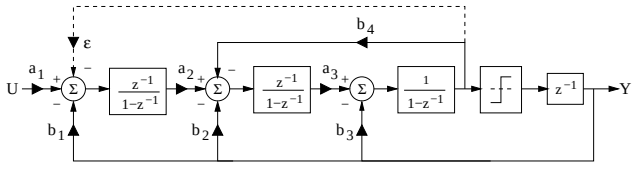

Figure 3: Block diagram of 3^{rd} order DSM with additional feedback ϵ to prevent cyclic output patterns.

Figure 3 shows a common 3^{rd} order modulator architecture, which has been complemented by an additional feedback path ϵ. The $[\mathbf{A}-\mathbf{I}]$ matrix of this modified 3^{rd} order system turns out to be

$$[\mathbf{A}-\mathbf{I}]_3 = \begin{bmatrix} 0 & 0 & -\epsilon \\ a_2 & 0 & -b_4 \\ a_2 a_3 & a_3 & -a_3 b_4 \end{bmatrix} \quad (13)$$

As can be seen, the additional feedback ϵ guarantees that the above matrix maintains rank N=3. In contrast to the 2^{nd} order example, however, where the additional path improved the noise shaping property, the feedback ϵ will degrade the noise suppression of this 3^{rd} order system. To find an expression for the expected loss, we have inspected the modified noise transfer function (NTF). Since the resulting noise suppression is almost exclusively determined by the numerator of the NTF, we will only list this polynomial. The corresponding z-domain function is

$$N_3(z) = (1-z^{-1})(1-z^{-1}[2-a_3 b_4]+z^{-2}) + \epsilon a_2 a_3 z^{-2} \quad (14)$$

The last term in the above equation indicates that the additional feedback ϵ creates an undesired leakage path for the quantization error. In order to minimize the resulting loss in noise suppression, ϵ must be chosen just large enough to prevent tonal patterns. Since we cannot express this optimization problem in simple mathematical terms, we have deduced the optimum value for the coefficient ϵ via a numerical simulator. The results of this optimization procedure will be presented in the next section.

4. NUMERICAL RESULTS

To reveal the impact of the proposed topological modifications, we have carried out various numerical simulations with the two example circuits shown in the previous section. The applied loop filter coefficients of the two systems are listed in table 4. Note that the given values represent a compromise between stability, noise shaping efficiency and dynamic range.

Coeff.	2^{nd} Order System	3^{rd} Order System
a_1	1/3	1/5
a_2	3/4	5/16
a_3	-	2/3
b_1	1/3	1/5
b_2	1/2	5/16
b_3	$4/9(\pi/OSR)^2$	2/3
b_4	-	$9/10(\pi/OSR)^2$

Table 1: Coefficient values of the two exemplary modulator topologies.

In all tonal simulations, we have assumed an idle input, since this is a frequently occurring situation in a practical application (e.g. a pause between words in an audio recording system). To avoid any correlation among the many output sequences, we started each simulation with a different initial state vector $\mathbf{x}(0)$ by using random values in the range ± 0.1. To exclude any residual transients, we have ignored the first 50,000 samples of each output vector. The patterns have been detected via an autocorrelation function. To investigate the two original topologies, we applied a frame length of 5,000 clock periods. This provided as with tonal frequencies as low as f_s/5,000. In case of the modified topologies, we had to reduce the window length to 1,000 periods, since we observed that the number of tones drastically diminished with increasing frame length. We attribute this observation to the relatively short lifetime of the remaining cyclic patterns. Recall that for any practical sampling rate in the MHz range, even a lifetime of 1,000 periods translates into a duration of a fraction of a millisecond. This renders the few *surviving* patterns very elusive. However, these temporary phenomena can still harm the dynamic range.

To obtain statistically significant numbers from the above described numerical pattern search procedure, we have simulated each modulator configuration 1,000 times.

In addition to detecting tonal patterns, we have also evaluated the maximum SNDR of each topology via a 2^{16} point FFT. To obtain a reliable SNDR value, we have averaged the results of 4 simulations carried out with 4 different sinusoidal inputs spanning the entire modulator passband range. Each input signal possessed a normalized amplitude of 0.5, or a power of -9 dB, respectively.

Figure 4 shows two possible responses of a single-stage 3^{rd} order DSM to a DC input. One response reflects the system while trapped in a limit cycle. Consequently, the spectrum consists of a train of discrete tones. The other response displays the alternative random quantization noise spectrum shaped by the NTF of the modulator to minimize the passband noise power. While both cases yield a similar total in-band quantization noise power of approximately -104 dB, it is obvious that the random noise response will be preferred since it enables a higher SFDR.

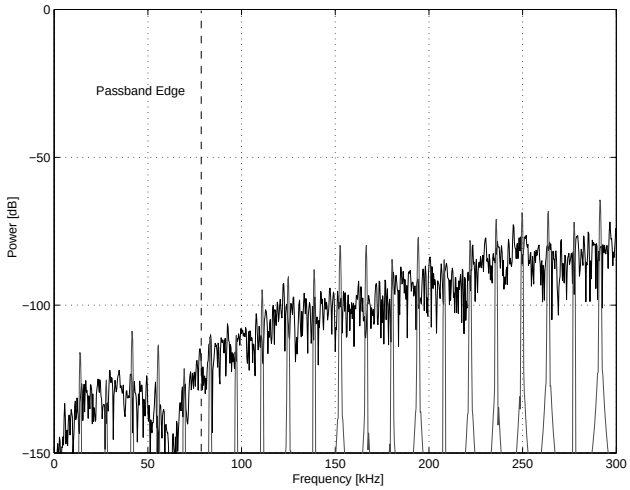

Figure 4: Typical quantization noise spectrum of a single-stage 3^{rd} order DSM for a DC input superimposed with a possible cyclic response of the same system.

Table 2 summarizes the numerical results we obtained from our exemplary 2^{nd} order system (cf. figure 2).

The values listed in this table clearly demonstrate the efficiency of the proposed limit cycle prevention procedure. For the

OSR	coeff. b_3	Passband Tones		$SNDR_{Max}$ [dB]	
		orig.	with b_3	orig.	with b_3
64	1.10×2^{-10}	835	0	69.8	73.3
96	1.95×2^{-12}	757	0	79.3	83.1
128	1.10×2^{-12}	674	4	85.8	88.9

Table 2: Detected tonal patterns among 1,000 simulation runs and maximum SNDR of 2^{nd} order DSM with and without additional feedback b_3.

two lower OSR values, the additional feedback path b_3 has eliminated all cyclic patterns. For the OSR of 128, the number of detected patterns has been reduced from several hundred to merely 4. The reason for the not entirely successful prevention of cyclic patterns in the latter case is the fact that b_3 must shrink as the square of the OSR to keep the passband noise power at a minimum (cf. equation 12). However, as expected, all three modified systems display an approximately 3.5 dB higher peak SNDR value.

As stated previously, our main objective in investigating the 3^{rd} order system has been to find the optimum value for the additional feedback path ϵ, i.e., the smallest value that effectively prevents tonal patterns. To obtain some meaningful results, we have simulated the system for three *typical* OSR values. In each case, we have logarithmically incremented ϵ by factors of 2. In addition, we have also evaluated the resulting penalty in the maximum SNDR. The numerical results are listed in table 3.

OSR	ϵ	Passband Tones	$SNDR_{Max}[dB]$
48	0	390	81.2
	2^{-15}	4	80.8
	2^{-14}	0	80.6
64	0	305	89.3
	2^{-16}	1	89.2
	2^{-15}	0	89.0
80	0	283	96.6
	2^{-17}	1	96.2
	2^{-16}	0	96.5

Table 3: Detected tonal patterns among 1,000 simulation runs and maximum SNDR of 3^{rd} order DSM for various OSR and ϵ values.

When viewing the values listed in table 3, it is important to mention that the additional feedback ϵ not only drastically reduced the number of cyclic patterns, but also diminished their survival rate. In fact, if we extended the tonal search procedure over a window length of 2,500 clock periods, no cyclic patterns were to be found any more. Table 3 also reveals that the minimum ϵ values required to prevent the occurrence of limit cycles turned out to be very small. Consequently, the resulting penalty in the maximum SNDR proved to be inconsequential. While this represents are very welcome result, the small ϵ values may limit the application of the proposed method to digital circuitry, since it is difficult to implement such small coefficients by analog means (e.g due to the resulting large coefficient spread). In addition, in case of frequently utilized switched-capacitor circuits, the small sampling capacitor implementing ϵ or the additional feedback coefficient b_3 would generate a prohibitive amount of kT/C noise. On the other hand, analog techniques possess a natural passive dithering scheme in form of thermal noise. If the power of the equivalent thermal noise source is on the order of the total in-band quantization noise, tonal patterns are very unlikely to occur. For example, if a designer targets a dynamic range of approximately 100 dB with an OSR of 64, a tonal free performance would require the input sampling capacitor to be smaller than 1 pF.

5. CONCLUSIONS

By utilizing state space matrix notation, we have shown that the likelihood of encountering limit cycles in DSM systems, when connected to a DC input, can directly be linked to a property of the system matrix **A**. Provided matrix **A-I** maintains rank N, the chances for encountering cyclic output patterns will be extremely low. In case the original **A** matrix fails to satisfy this condition, we have shown that it is possible to achieve an excellent limit cycle immunity by simply adding another feedback path to the modulator loop filter. In contrast to previous limit cycle suppression techniques, the proposed topological modifications are readily implemented, at least in a digital system, without visibly penalizing the system's SNDR. In fact, the modified 2^{nd} order DSM performs even slightly better than the original system by yielding a 3.5 dB higher SNDR.

6. REFERENCES

[1] S. Hein and A. Zakhor, "On the stability of sigma-delta modulators," *IEEE Transaction on Signal Processing*, vol. 41, pp. 2322–2348, July 1993.

[2] S. I. Mann and D. P. Taylor, "Limit cycle behavior in the double-loop bandpass sigma-delta A/D converter," *IEEE Transaction on Circuits and Systems–Part II*, vol. 46, pp. 1086–1089, Aug. 1999.

[3] V. Friedman, "The structure of the limit cycles in sigma-delta modulation," *IEEE Transaction on Communications*, vol. 36, pp. 972–979, Aug. 1988.

[4] S. R. Norsworthy, "Effective dithering of sigma-delta modulators," in *Proceedings of International Symposium on Circuits & Systems*, pp. 1304–1307, 1992.

[5] R. Schreier, "Destabilizing limit cycles in delta-sigma modulators with chaos," in *Proceedings of International Symposium on Circuits & Systems*, pp. 1369–1372, 1993.

[6] L. Risbo, "On the design of tone-free $\Sigma\Delta$ modulators," *IEEE Transaction on Circuits and Systems–Part II*, vol. 42, pp. 52–55, Jan. 1995.

[7] M. Motamed, A. Zakhor, S. Sanders, and T.-W. Lee, "Spectral characteristics of the double-loop sigma-delta modulator," *IEEE Transaction on Circuits and Systems–Part II*, vol. 45, pp. 144–147, Jan. 1998.

[8] G. Fischer and D. Hyun, "Limit cycles in single-stage delta-sigma modulators," in *Proceedings of International Symposium on Circuits & Systems*, vol. 2, pp. 376–379, 1999.